Deep-level Trap Formation in Si-Substituted $Sr_2SnO_4:Sm^{3+}$ for Rewritable Optical Information Storage

Jiaren Du, Shaoxing Lyu , Kai Jiang , Dong Huang , Jiang Li , Rik Van Deun, Dirk Poelman, Hengwei Lin**

Dr. Jiaren Du, Shaoxing Lyu , Dr. Kai Jiang , Prof. Hengwei Lin
International Joint Research Center for Photo-responsive Molecules and Materials, School of Chemical and Material Engineering, Jiangnan University, 214122, Wuxi, China.
E-mail: Dr. Jiaren Du (jiaren.du@jiangnan.edu.cn)
Prof. Hengwei Lin (linhengwei@jiangnan.edu.cn)

Dong Huang , Prof. Jiang Li
Key Laboratory of Transparent Opto-functional Inorganic Materials, Shanghai Institute of Ceramics, Chinese Academy of Sciences, Shanghai 201899, China.

Prof. Rik Van Deun
L^3–Luminescent Lanthanide Lab, Department of Chemistry, Ghent University, Krijgslaan 281-S3, B-9000 Ghent, Belgium.

Prof. Dirk Poelman
LumiLab, Department of Solid State Sciences, Ghent University, Krijgslaan 281-S1, B-9000, Ghent, Belgium.
Center for Nano- and Biophotonics (NB-Photonics), Ghent University, B-9000, Ghent, Belgium.

Keywords: deep trap, persistent luminescence, co-doping, optical information storage, rare-earth doped materials

Abstract: Persistent luminescent materials containing deep-level traps have attracted extensive research interest in the field of optical information storage due to their unique features of long-lasting emission, energy storage and controllable photon release upon external stimulations. However, the lack of suitable luminescent materials with deep-level traps is still the bottleneck of such an optical storage application. Herein, we report a series of persistent luminescent materials with reddish-orange emissions and controllable photon release upon thermal stimulation. Through substitution of Sn by Si, more and deeper trap levels are achieved in $Sr_2SnO_4:Sm^{3+},Si^{4+}$ phosphors. Moreover, both ultraviolet light and high-energy X-ray irradiations can induce reddish-orange emitting persistent luminescence from the as-synthesized samples. Rewritable optical information storage and readout based on photon trapping and de-trapping processes are demonstrated. Optical information can be handily encoded using a commercially available 365 nm light emitting diode, and decoded upon thermal stimulation. The $Sr_2SnO_4:Sm^{3+},Si^{4+}$ phosphors as presented in this work show a great promise for rewritable optical data storage and information encryption.

1. Introduction

Information storage has played an indispensable role in the evolution of human’s history. With the development of Internet of Things, an extremely large amount of digital data is being produced by computers, smartphones, sensors and automobiles. It has been proposed that the volume of digital data doubles every two years, and the big data era requires large storage resources and suitable processing media[1, 2, 3]. Compared to many other information storage technologies, optical information storage, as an emerging technology, exhibits the merits of ultra-high capacity, ultra-long lifetime, ultra-low power consumption, re-writability and erasability[4]. More impressively, multiplexing optical information storage provides an exceptional approach to greatly improve the storage capacity by expanding the two-dimensional space towards multidimensional spaces, such as multiplexing of wavelength, intensity and time gate[5, 6, 7, 8, 9]. However, the lack of suitable optical storage media is still the bottleneck of such optical storage technologies, hindering their practical application. Therefore, the development of novel advanced optical materials combining several luminescence features is urgently needed to handle these challenges.

Persistent luminescent materials, as one specific member in the family of advanced optical materials, have been widely applied in the fields of glow-in-the-dark paints, night-vision surveillance, in vivo bio-imaging, alternating current light emitting diodes, emergency signage, information security and optical data storage[10, 11, 12, 13, 14, 15]. The high energy-storage capacity and long-lasting emission lifetime provide persistent luminescent materials with remarkable advantages in the above-mentioned fields. In regard to the practical applications of optical information storage, the Mn^{2+} or Cr^{3+} doped $LiGa_5O_8$ persistent phosphors have been proposed as excellent optical storage media due to their intensity or wavelength multiplexing[16, 17]. Recently, $NaLuF_4:Tb^{3+}@NaYF_4$ nano-scintillators have been reported as high-resolution 3D X-ray extension imaging storage media that can trap high-energy X-rays for weeks[18]. Zhuang et al. have developed a series of $(Sr_{1-x}Ba_x)Si_2O_2N_2$:Eu/Yb,Dy persistent luminescent materials with deep-lying traps and demonstrated their feasibility as optical data storage media and information security system[7]. Despite these progresses, only a handful of candidates have been reported as optical data media among the large number of persistent luminescent materials so far. To date, the exploration of materials for information storage is usually based on a trial-and-error approach. It is quite essential to develop new optical materials combining both persistent luminescence and high energy-storage capacity in a designed way.

Co-doping or chemical substitution, including chemical unit co-substitution, neighboring-cation substitution and cation-size-mismatch, have been regarded as effective and facile strategies in luminescent materials for solid-state lighting[19, 20]. By co-doping specific ions, the regulation of the surrounding environment of emitting centers or the formation of new trap levels plays an important role in tailoring the optical properties of solid-state lighting phosphors or persistent luminescent materials[21, 22, 23, 24, 25]. For instance, co-doping $LiGa_5O_8:Cr^{3+}$ with Si^{4+} or Ge^{4+} ions has been investigated by Poelman et al., and it was reported that the persistent luminescence was significantly improved and the number of deep-lying traps was increased[26].

Upon defect engineering and reducing the Si content, single-component white-light $NaLi_3Si_{1-x}O_4:Eu^{2+}$ materials with broad-band defect-induced charge-transfer emission were designed[24]. By selecting different lanthanide co-dopants, Xie and co-workers developed a series of deep-trap persistent luminescent materials in the $SrSi_2O_2N_2:Ln^{2+},Ln^{3+}$ system[6]. Furthermore, an improvement of the persistent luminescence of near-infrared emitting $ZnGa_2O_4:Cr^{3+}$ phosphor has been made by employing various co-dopants, such as Ge, Sn or Bi ions[10, 27, 28]. Recently, Liu et al. successfully tailored multi-dimensional triple traps through co-doping Tb^{3+} ions into Pr^{3+}-activated Y_2GeO_5 phosphors for binary optical data storage[29]. It is clear that the introduction of trap energy levels (i.e., both the position and the amount of trap energy levels), especially the formation of more deep-trap levels, is of great significance in the design of optical information storage materials. To obtain deep-lying traps for the design of new storage phosphors, band-gap engineering or trap-level engineering is often employed by appropriately screening co-dopants.

In this work, for the first time, deep-trap reddish-orange emitting persistent luminescent $Sr_2SnO_4:Sm^{3+},Si^{4+}$ phosphors were successfully developed through a chemical substitution approach. Both ultraviolet (UV) light and high-energy X-ray irradiation can induce persistent luminescence from the as-synthesized phosphors. Moreover, these materials exhibit reversible photochromism upon alternating illumination (365 nm) and thermal stimulus (300 °C). By Si ions substitution, formation of deep-level traps is achieved in $Sr_2SnO_4:Sm^{3+},Si^{4+}$ phosphors, which shows promise for rewritable optical information storage. Based on photon trapping and de-trapping processes, rewritable optical data storage and readout was demonstrated. Patterned information is handily encoded by a commercially available 365 nm light emitting diode, and the recorded optical data is decoded by means of thermal stimulus. The deep-level trap persistent luminescent phosphor as presented in this work not only shows a great promise for rewritable optical information storage and data encryption, but also provides guidance to design other deep-trap-containing optical materials.

2. Material and Methods

2.1. Materials Preparation

The $Sr_{2-x}Sn_{1-y}O_4$:$x$$Sm^{3+}$,$y$$Si^{4+}$ phosphors were prepared using a high-temperature solid-state reaction method. Dopants Sm^{3+} and Si^{4+} were added as Sm_2O_3 and SiO_2, respectively. The stoichiometric number x was chosen from 0.005 to 0.04, and y was chosen from 0.025 to 0.25. The appropriate stoichiometric amounts of $SrCO_3$ (Aladdin, 99.995%), SnO_2 (Innochem, 99.99%), SiO_2 (Aladdin, 99.99%), Sm_2O_3 (Aladdin, 99.99%) were weighed. Precursors were mixed with ethanol and ground thoroughly in an agate mortar. To make a homogeneous mixture, repeated grinding was performed for 1 hour. The mixtures were dried in an oven at 50 °C and added with a 5 wt% polyvinyl alcohol (PVA) binder solution, then pressed into pellets with a thickness of about 1.5 mm by applying a uniaxial pressure of 200 MPa. Subsequently, these pellets were sintered at 700 °C for 6 h in air to remove the PVA residues and then kept at 1300 °C for 8 h. The employed heating rate for all samples were 300 °C/h using a tube furnace (KTL1700-80, Nanjing Laibu Tech.), and the prepared samples were allowed to cool down naturally overnight. The samples were well ground again manually for further characterization. The chemical composition of $Sr_{2-x}Sn_{1-y}O_4$:$x$$Sm^{3+}$,$y$$Si^{4+}$ (x= 0.01, y= 0.05) was chosen as an example discussed in this work.

2.2. Structure and Morphology Characterization

X-Ray powder diffraction (XRD) were recorded on an X-ray powder diffractometer (D8, Bruker AXS, Germany) using Cu Kα (1.5406 Å) radiation at room temperature. The XRD data were collected with a 0.02° step size and 1.5 s integration step time in the range 2θ from 10° to

80°. The measured XRD patterns were compared with the standard data (PDF No.74-1348) from the structure of the corresponding Sr_2SnO_4 host matrix. The morphology and elemental distribution mappings of samples were characterized via a thermal field emission scanning electron microscope (Verios G4 UC) equipped with an EDS analysis system (Thermo Scientific, U.S.A.).

2.3. Luminescence Characterization

Photoluminescence excitation, emission spectra, persistent luminescence decay curves were obtained by a fluorescence spectrometer (FS5, Edinburgh, UK) equipped with a 450 W xenon arc lamp at room temperature. All spectra were automatically corrected for detector response. Persistent luminescence excitation spectrum was collected upon monitoring afterglow emission at 646 nm. After charging for 2 minutes, the integrated persistent luminescence intensity was plotted as a function of the charging wavelength by integrating the decay profiles during the first minute of afterglow. Monochromatic light ranging from 280 to 560 nm from a 450 W xenon arc lamp was used as excitation source. Temperature-dependent photoluminescence spectra were collected in the temperature range of 30-150 °C by a portable spectrometer (Ocean Optics). Diffuse reflection spectra were measured by using a UV-VIS-NIR spectrophotometer (SHIMADZU UV-3600 Plus) with a step size of 0.5 nm in scanning range from 200 nm to 1000 nm. For photochromism measurements, diffuse reflection spectra were collected after 30-second thermal treatment at various temperatures from 50 °C up to 300 °C. Reversible photochromism tests were performed upon alternating illumination (365 nm) and thermal stimulus (300 °C). Radioluminescence and temperature dependent emission were collected by an optical fiber connected to a spectrometer (Ocean Optics). A commercial 254 nm UV lamp, 365 nm light emitting diode or software-controlled X-ray tube (70 kV, 1.5 mA) was used as irradiation source. TL measurement was performed by a FJ-427A1 thermo-luminescence dosimeter (Beijing Nuclear Instrument) with a constant heating rate of 1 °C/s.

2.4. Applications in Optical Data Storage

The samples of $Sr_2SnO_4:Sm^{3+},Si^{4+}$ were ground manually for 30 minutes. Subsequently, 25 mL commercial printing ink was mixed with 0.5 g fine powder of $Sr_2SnO_4:Sm^{3+},Si^{4+}$. The mixture was well mixed by 20-minute ultrasonic treatment and 30-minute mechanical stirring, and the as-obtained homogeneously dispersing suspension was used as luminescent ink for screen-printing. Text information of Chinese ideographs was printed on a piece of A4 paper using the luminescent ink. Commercial flat printing screen and brush were used, and the printed paper was fully dried overnight at room temperature. The temperature-controlled heating platform (maximum at 300 °C) or a domestic electric hair drier (using the maximal heating mode) was applied as heating source. Photographs of the printed text patterns were taken using a mobile phone (Huawei).

3. Results and Discussion

3. 1. Crystalline Phase and Photoluminescence Property

A series of $Sr_{2-x}Sn_{1-y}O_4:xSm^{3+},ySi^{4+}$ ($0.005 \leq x \leq 0.04$, $0.025 \leq y \leq 0.25$) phosphors were prepared and the chemical compositions of $Sr_{2-x}SnO_4:xSm^{3+}$ ($x = 0.01$) and $Sr_{2-x}Sn_{1-y}O_4:xSm^{3+},ySi^{4+}$ ($x = 0.01$, $y = 0.05$) were selected for a detailed analysis and discussion as examples (see Experimental Section). X-ray diffraction (XRD) and scanning electron microscopy (SEM) measurements were employed to investigate the crystal structure and morphology of $Sr_2SnO_4:Sm^{3+}$ and co-doped $Sr_2SnO_4:Sm^{3+},Si^{4+}$ samples. XRD patterns of $Sr_2SnO_4:Sm^{3+}$ and $Sr_2SnO_4:Sm^{3+},Si^{4+}$ are shown in Figure 1(a). Both patterns are fully consistent with the standard pattern of the Sr_2SnO_4 host matrix (PDF card No.74-1348). A small amount of Sm^{3+} ions doping or Sm^{3+}-Si^{4+} co-doping does not induce any noticeable changes in the XRD patterns. There were no obvious impurity or secondary phases observed in XRD patterns and the main diffraction peaks were sharp and intense, indicating high crystallinity and feasible incorporation of Sm^{3+} and Si^{4+} dopants into the host. The schematic crystal structure diagram of the Sr_2SnO_4 host is given in Figure S1. Sr_2SnO_4 with space group *I4/mmm* (139) shows a tetragonal symmetry with a K_2NiF_4-type structure[30]. It is reported that tailoring trap defects is uncomplicated in the case of the quasi-two-dimensional Sr_2SnO_4 structure, and this quasi-two-dimensional structure is composed of corner-shared SnO_6 octahedral units[30]. Trivalent samarium (Sm^{3+}) and tetravalent silicon (Si^{4+}) ions are supposed to substitute divalent strontium (Sr^{2+}) and tetravalent tin (Sn^{4+}) sites, respectively, due to their similar coordination environment, ionic radius and valence states. Figure 1(b) and Figure S2 show the SEM images of Sr_2SnO_4:Sm^{3+},Si^{4+} sample, in which the particle size is in the micrometer range (around 5 μm) with high crystallinity. Moreover, to confirm the composition uniformity of Sr_2SnO_4:Sm^{3+},Si^{4+} sample, energy dispersive X-ray spectroscopy (EDS) elemental mapping analysis was performed in a selected area (see Figure 1(b) for the selected EDS elemental mapping area). Elements Sr, Sn, O, Sm and Si are homogeneously distributed within the measured particles from these elemental mapping images in Figure 1(c)-(g). Also, SEM images with EDS elemental mappings of Sr_2SnO_4:Sm^{3+}, are shown in Figure S3 and S4. All these SEM-EDS results support the high purity of the Sr_2SnO_4 crystalline phase in accordance with the XRD data.

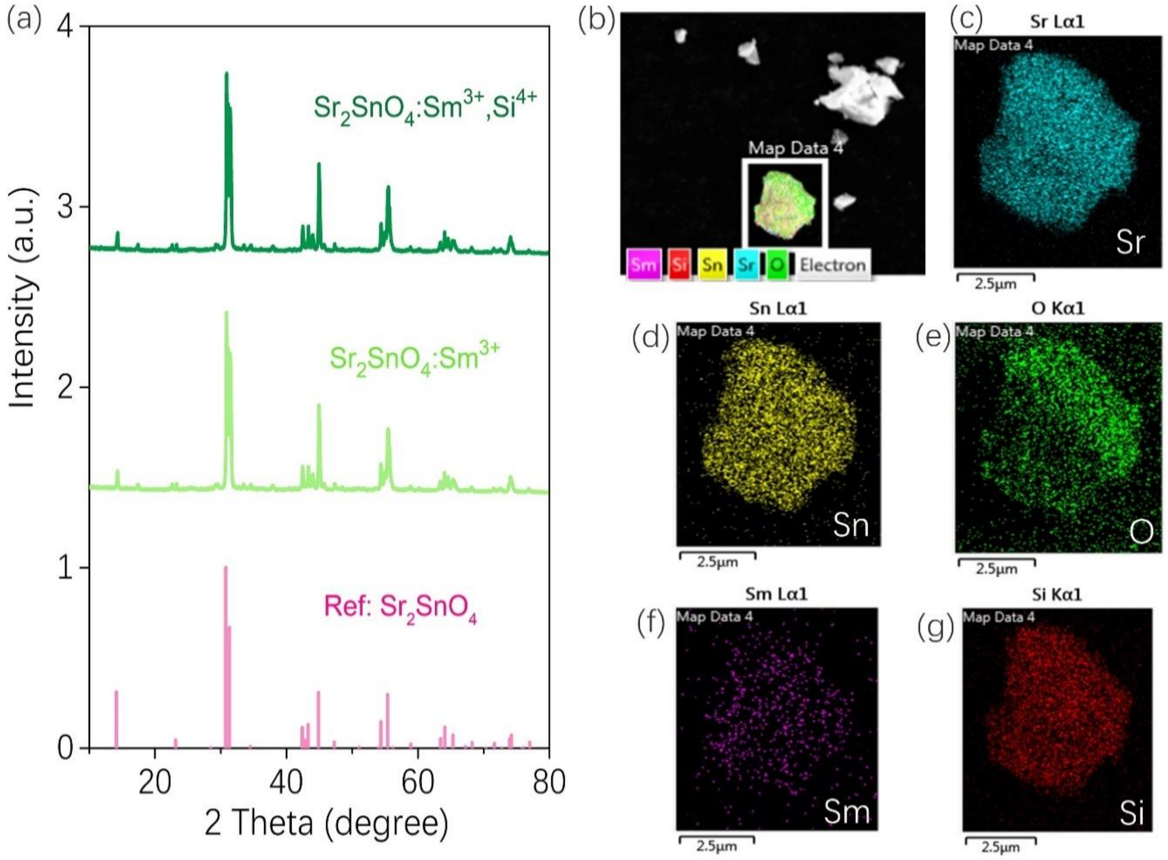

Figure 1. (a) XRD patterns of Sr_2SnO_4:Sm^{3+}, Sr_2SnO_4:Sm^{3+},Si^{4+} sample and standard reference of Sr_2SnO_4 host (No.74-1348); (b) SEM image of Sr_2SnO_4:Sm^{3+},Si^{4+} particles and the selected EDS elemental mapping area; (c)-(g) EDS elemental mapping images of Sr, Sn, O, Sm and Si for the selected Sr_2SnO_4:Sm^{3+},Si^{4+} particle. All the scale bars are 2.5 μm in the elemental mapping images (c-g).

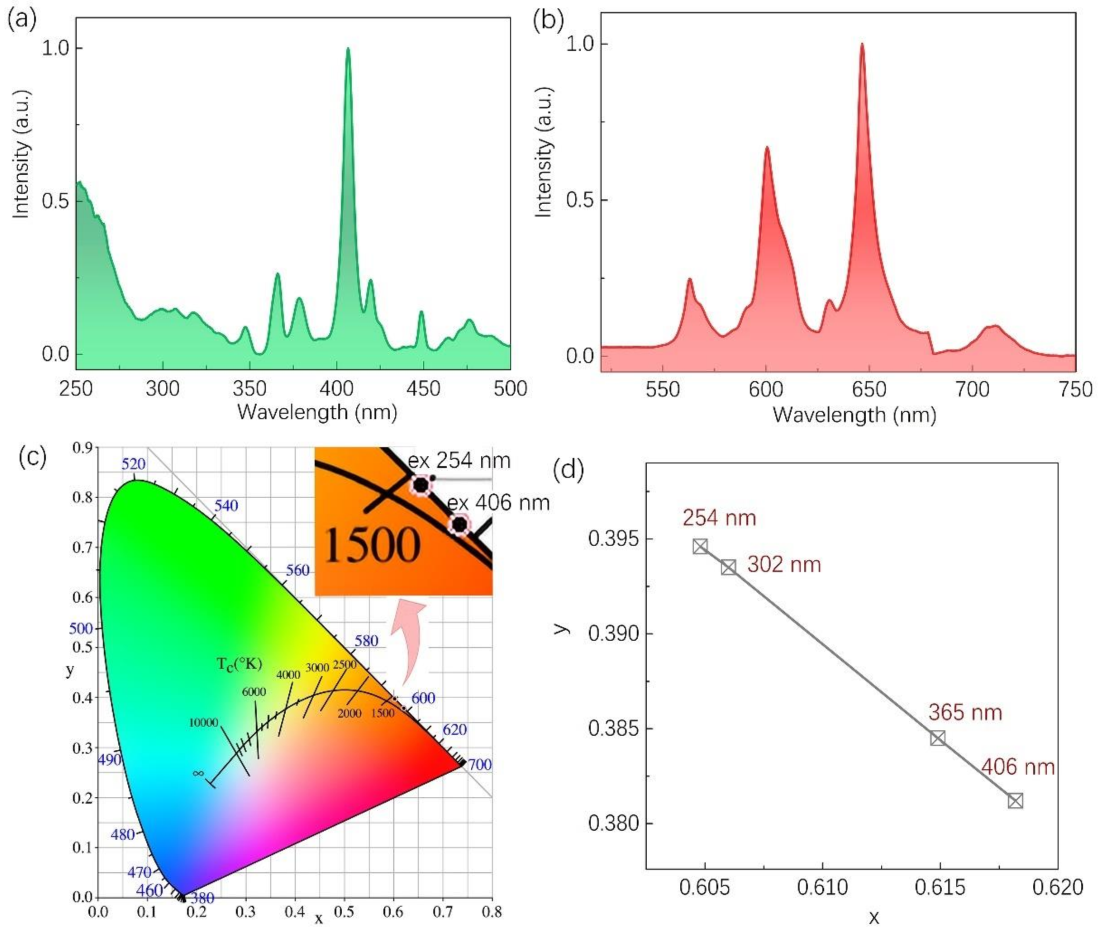

Figure 2. (a) Photoluminescence excitation spectrum of Sr_2SnO_4:Sm^{3+},Si^{4+} (λ_{em}= 646 nm) ; (b) Photoluminescence spectrum of Sr_2SnO_4:Sm^{3+},Si^{4+} (λ_{ex}= 406 nm); (c) Excitation wavelength dependent CIE chromaticity diagram of Sr_2SnO_4:Sm^{3+},Si^{4+}, and the inset is the enlarged area of the target chromaticity diagram; (d) Comparison of chromatic coordinates under 254, 302, 365 and 406 nm excitation.

The photoluminescence excitation (PLE) and photoluminescence (PL) spectra of Sr_2SnO_4:Sm^{3+},Si^{4+} are shown in Figure 2(a) and (b), respectively. The PLE spectrum, monitored at 646 nm (λ_{em}= 646 nm), exhibits numerous peaks ranging from 250 nm to 450 nm, indicating that the as-prepared sample can be excited by UV to blue light. The intense broad bands together with several band shoulders located at shorter wavelength range (250- 340 nm) can be assigned to the overlap of the Sr_2SnO_4 host absorption and the charge transfer transition between O^{2-} and Sm^{3+}. The narrow peaks can be attributed to intra-configurational *4f*-*4f* transition of Sm^{3+}, consistent with previous literatures[30, 31]. The maximum of the excitation spectrum due to the overlap between the fundamental host absorption and the charge transfer band has been reported to be around 247 nm, out of the wavelength range of the measured PLE spectrum due to experimental limitations[30]. Furthermore, there are many narrow excitation peaks in the wavelength range from 340 nm to 500 nm, as illustrated in Figure 2(a). The main excitation peaks are centered at 347.5 nm, 366 nm, 378.5 nm, 406 nm, 419.5 nm, 448.5 nm, 464 nm, and 477 nm. These sharp peaks observed in Figure 2(a) can be attributed to the *4f*-*4f* electronic transitions of Sm^{3+}, that is, from ground state $^6H_{5/2}$ to the excited state $^4H_{9/2}$, $^4D_{3/2}$, $^4D_{1/2}$, $^4F_{7/2}$, $^6P_{5/2}$, $^4G_{9/2}$, $^4I_{13/2}$, $^4I_{11/2}$, respectively[32, 33]. The features of the PLE bands are similar to those from reports by Luo et al. in $Sr_2SnO_4:Sm^{3+}$ ceramics, with slight variations of wavelength values[33]. As shown in Figure 2(a), the strongest excitation band is located at 406 nm, from the $^6H_{5/2} \rightarrow {}^4F_{7/2}$ transition of Sm^{3+}. It is worth mentioning this excitation band matches well with the light output from commonly available near-UV chips in solid-state lighting industry, suggesting $Sr_2SnO_4:Sm^{3+},Si^{4+}$ investigated in the present work may find its application in phosphor-converted white light emitting devices. Upon excitation at 406 nm (λ_{ex}= 406 nm), the PL spectrum of $Sr_2SnO_4:Sm^{3+},Si^{4+}$ in Figure 2(b) shows the typical emission transitions of Sm^{3+}, which are due to the intra-*4f* transitions from the excited energy level ($^4G_{5/2}$) to lower levels (^6H_J, J= 5/2, 7/2, 9/2, 11/2). The four main emission peaks are centered at 563 nm ($^4G_{5/2} \rightarrow {}^6H_{5/2}$), 600.5 nm ($^4G_{5/2} \rightarrow {}^6H_{7/2}$), 646 nm ($^4G_{5/2} \rightarrow {}^6H_{9/2}$) and 711 nm ($^4G_{5/2} \rightarrow {}^6H_{11/2}$), respectively. As a comparison, excitation-wavelength dependent emission spectra are presented in Figure S5. When excited at shorter wavelengths, the energy level splitting effect is found more clearly. The relative intensity and position of PL bands are also changing with varying the excitation wavelengths, which indicates the dominant intra-*4f* transitions are excitation-wavelength dependent. It can be seen that all these sharp emission lines together make the phosphor reddish-orange, and the Commission Internationale de L'Eclairage (CIE) diagram of $Sr_2SnO_4:Sm^{3+},Si^{4+}$ is presented in Figure 2(c). Upon excitation at different wavelengths, a tiny difference of the CIE chromaticity diagram and corresponding chromaticity coordinates is observed in Figure 2(c) and (d), respectively. As a result, the combined emission color shifts slightly within the reddish-orange region. The chromatic coordinates displayed in Figure 2(d) also show approximately a linear change with varying excitation wavelengths from 254 nm to 406 nm. This means the sample presents a small excitation-wavelength dependent color change.

3.2. UV and X-rays Excited Persistent Luminescence

Apart from the steady-state luminescence discussed above, $Sr_2SnO_4:Sm^{3+},Si^{4+}$ also exhibits persistent luminescence. Photographs of the sample were taken under daylight, laboratory UV lamp (λ_{ex}= 365 nm), and in a dark-box (after ceasing UV excitation for 5, 30, 60, and 90 seconds). As shown in Figure 3(a), reddish-orange emission can be observed by the naked eyes for tens of seconds after switching off the 365 nm UV lamp. Moreover, a persistent luminescence decay profile was recorded at room temperature, shown in Figure 3(b). The logarithmic plot of the afterglow intensity as a function of time shows that the intensity is monotonically decreasing. The decay rate which corresponds to the slope of curve is related to the structure of traps and deeper electron traps may cause a slower de-trapping rate. The power law dependence of the decay curve on a log/log plot seen in Figure 3(b), indicates there are many individual traps with different trap depth controlling the persistent luminescence[34, 35]. The persistent luminescence excitation spectrum (PLES) of $Sr_2SnO_4:Sm^{3+},Si^{4+}$ is recorded in Figure S6 upon monitoring afterglow emission at 646 nm. After charging for 2 minutes, the integrated persistent luminescence intensity was plotted as a function of the charging wavelength by integrating the decay profiles during the first minute of afterglow. From PLES, it can be seen that the charging wavelength at UV range is most effective for inducing persistent luminescence. A blue light emitting diode at a wavelength higher than 420 nm cannot induce persistent luminescence. The band gap of the Sr_2SnO_4 was measured to be 4.49 eV[36], and there is a strong onset of absorption from around 400 nm. It should be noted that the host absorption spectrum closely matches the excitation spectrum for persistent luminescence seen in Figure S6. More impressively, reddish-orange persistent luminescence is detectable by the naked eyes in a dark-box after X-ray irradiation, which proves the ability to charge the persistent phosphor using high energy radiation and makes it possible to develop an X-ray responsive material. Persistent phosphors that can be charged by X-rays have been promising for deep-tissue ultrasensitive imaging, photodynamic therapy, and information storage. The radioluminescence (RL) spectrum and emission spectrum after cessation of X-ray irradiation are displayed in Figure 3(c) and (d). Although different spectrophotometers were used, the main spectroscopic features of Sm^{3+} during and after X-ray irradiation are similar, and comparable to emissions at an excitation wavelength of 254 nm and 302 nm (Figure S5). Moreover, the CIE diagram of the sample upon X-ray irradiation is given in Figure S7. The chromaticity coordinates of RL are also located in the reddish-orange region, showing the same emitting centers (Sm^{3+} ions). The long-lasting emission after X-ray irradiation indicates electron-trapping states are generated in the host lattice. Thus, trap filling by both UV light and high-energy X-rays is possible.

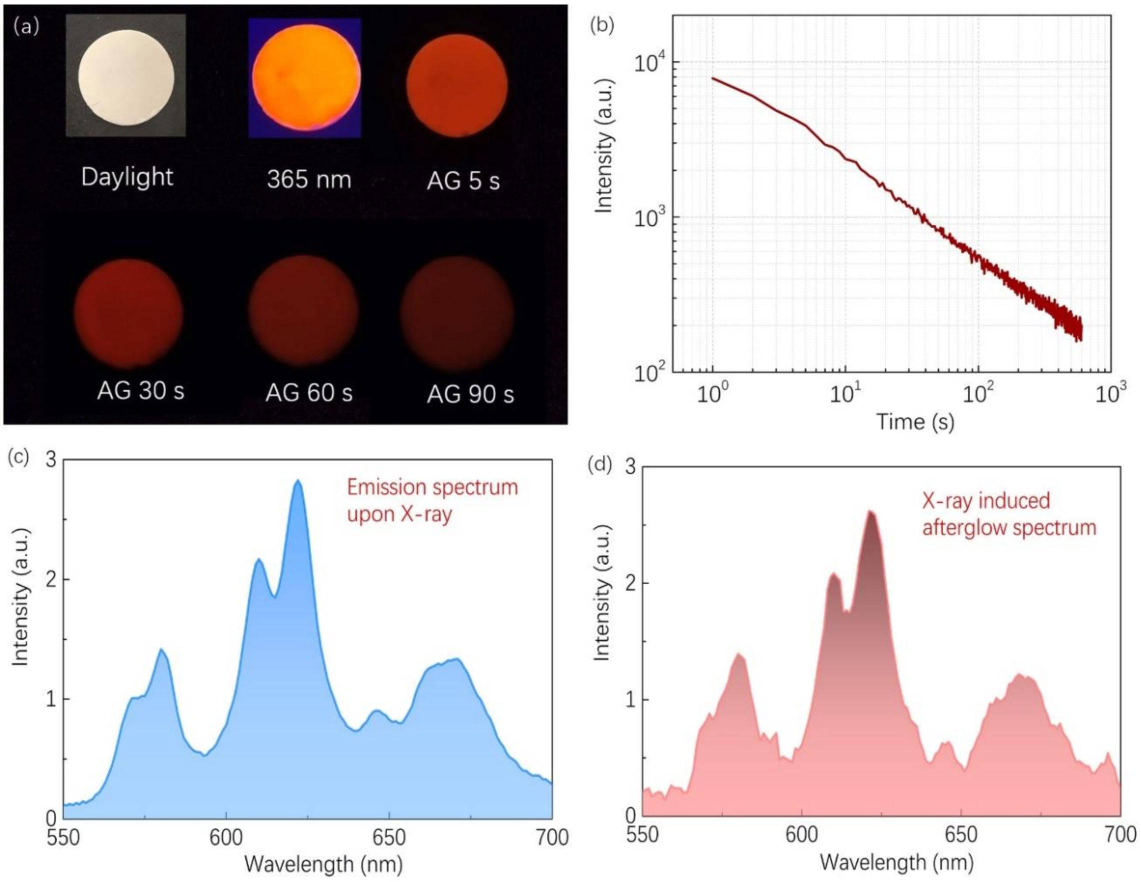

Figure 3. (a) Photographs of a $Sr_2SnO_4:Sm^{3+},Si^{4+}$ sample under daylight, laboratory UV lamp excitation (λ_{ex}= 365 nm), and in a dark-box after ceasing UV excitation (afterglow (AG) at 5 s, 30 s, 60 s and 90 s); (b) Room temperature persistent luminescence decay curve as a function of time; (c) Radioluminescence (RL) spectrum (X-ray tube at 70 kV, 1.5 mA); (d) Emission spectrum after cessation of X-ray irradiation.

3.3. Thermal Stability and Reversible Photochromism

A key parameter evaluating the luminescence performance for practical applications is the thermal stability. The thermal stability (or thermal quenching behavior) of the $Sr_2SnO_4:Sm^{3+},Si^{4+}$ is investigated in this part. Temperature-dependent PL spectra of $Sr_2SnO_4:Sm^{3+},Si^{4+}$ are shown in Figure S8 over a temperature range from 30 °C to 150 °C. To clearly see the differences between the spectral shapes, the absolute PL spectra and their corresponding normalized spectra at 30 °C, 80 °C and 150 °C, are compared in Figure S8(b) and Figure S9, respectively. Here, only the main emission lines are considered, which are ascribed to the intra-*4f* transitions of Sm^{3+} from the excited energy level ($^4G_{5/2}$) to lower levels (^6H_J, J= 5/2, 7/2, 9/2). Overall, the emission intensity decreases when increasing temperature, as expected, mainly due to the substantial increase in the non-radiative relaxation rate. It can be observed that the position and shape of emission peaks do not change, but the relative intensity of the different peaks varies with the increase of temperature. Thus, the temperature dependent behavior of each transition is clearly different. To further investigate the thermal quenching behavior, the relative intensities of temperature-dependent integrated PL spectra are presented in Figure S8(c). Interestingly, the integrated emission intensity of Sr_2SnO_4:Sm^{3+},Si^{4+} first increases in the initial temperature range from 30 °C to 80 °C, and then gradually drops to about half of the maximum at 150 °C.

Furthermore, reversible photochromism was observed by alternating illumination (using a commonly available in-lab 365 nm lamp) and thermal stimulus (via heating treatment on a temperature-controlled platform or an oven), as illustrated in Figure 4(a). This reversible white-grey color change (photochromism) can be connected to the emitting centers and defects from the Sr_2SnO_4 host lattices with layered perovskite-related structure units[37]. Photochromism has also been found in other Sr_2SnO_4 based systems doped by appropriate rare-earth ions (Er^{3+}, Eu^{3+}, Sm^{3+})[33, 37, 38, 39]. With the aid of the photochromic phenomenon, luminescence modulation was demonstrated. PL spectra were measured before and after 5-minute 365 nm illumination, as displayed in Figure 4(b). While there is no change in position and shape of the emission bands, the PL intensity decreases, in accordance with observations in previous literatures[33]. The ratio of emission intensity modulation before and after photochromism is 66.8 % and 67.3 % at the wavelength of 600.5 nm and 646 nm, respectively. Diffuse reflection spectra were recorded before (Initial) and after 365 nm illumination for different durations in

Figure 4(c). After illumination, the reflection intensity decreases in the visible wavelength range, which is the main reason for the greying of the sample. The gradual change of reflectance is not very large, resulting in a correspondingly mild luminescence modulation. Figure S10 gives the decrease of reflectivity (ΔR) as a function of wavelength after 300-second irradiation. There is an obvious narrow absorption peak at 406 nm, coming from the characteristic absorption of Sm^{3+} ions. The narrow peaks in the diffuse reflection spectra are consistent with those of the PLE spectrum in Figure 2(a). The photochromic phenomenon can be induced upon illumination for merely seconds, and further long-duration illumination does not contribute much to the color change as seen from Figure 4(c). For the de-coloration, diffuse reflection spectra of the colored phosphor (as colored grey state) after thermal treatment at different ambient temperatures (from 50 °C up to 300 °C) are shown in Figure 4(d). Notably, simply prolonging the fading time at room temperature or employing mild thermal stimulus (thermal temperature below 80 °C) cannot switch the sample back to its initial white-appearance (see Figure S11 and S12). A complete de-coloration process (the color returns to its original white state) could be achieved upon more ambient thermal energy, for example, heating up to 300 °C. All these observations may be related to the deep-trap energy levels within the host lattice[40], which is discussed in detail below.

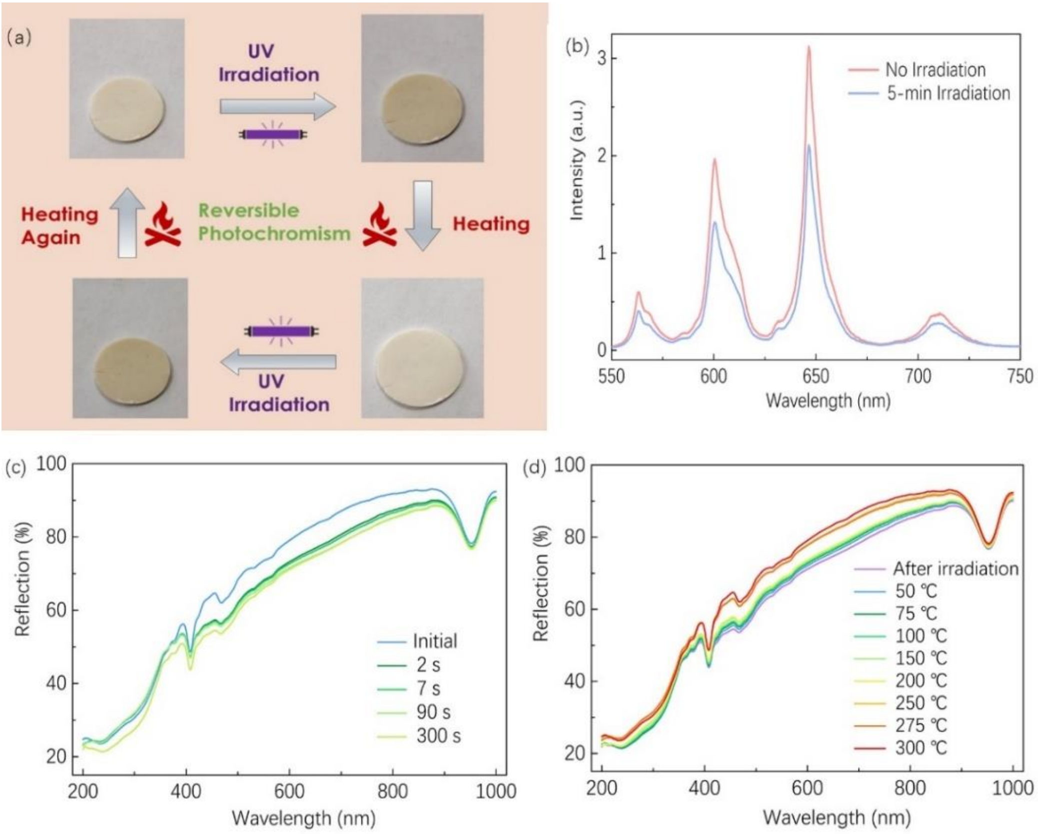

Figure 4. (a) Reversible photochromism upon alternating illumination (365 nm) and thermal stimulus (300 °C); (b) Luminescence modulation via 365 nm illumination; (c) Diffuse reflection spectra before (Initial) and after 365 nm illumination for different durations (irradiation for 2 s, 7 s, 90 s or 300 s); (d) Diffuse reflection spectra after 30-second thermal treatment at different temperatures (from 50 °C up to 300 °C).

3.4. Deep-level Trap Formation upon Si Substitution

To further evaluate the traps, thermoluminescence (TL) measurements were performed with the sample pre-irradiated by UV or X-rays. Figure 5(a) displays the obtained TL glow curves of $Sr_2SnO_4:Sm^{3+}$ (Sm^{3+}-curve) and $Sr_2SnO_4:Sm^{3+},Si^{4+}$ (Sm^{3+},Si^{4+}-curve) without fading between UV irradiation stage (10-minute irradiation) and heating stage. Also, the TL glow curve of $Sr_2SnO_4:Sm^{3+}$ after 10-minute fading at 70 °C is given (Sm^{3+} fading at 70 °C-curve). Here, the TL fading at 70 °C acts as a fast-thermal-cleaning step to empty the relatively shallow traps. For a clear illustration, the temperature range was roughly divided into three regions, that is, Region-I (in green, from room temperature to 90 °C), Region-II (in orange, from 90 °C to 175 °C), and Region-III (in red, from 125 °C to 240 °C). Broad TL intensity profiles were measured, and the strong TL signals at the start of the heating stage (Region-I) correspond to the persistent luminescence at room temperature, because no fading was employed between charging and heating stage. The energy of traps was distributed over a large range (covering Region I, Region II and Region III). These broad TL glow curves with shoulders and continuous signals at high temperatures and the wide distribution range of trap levels strongly suggest the presence of multiple, close-lying and deep trapping states in both $Sr_2SnO_4:Sm^{3+}$ and $Sr_2SnO_4:Sm^{3+},Si^{4+}$ phosphors. This result perfectly fits with the power law dependence of the decay curve seen in Figure 3b, as the latter also points at a wide distribution of traps controlling the persistent luminescence[35]. The trap parameters, such as trap depth and trap distribution, usually govern the shape of the TL glow curve, especially the position of the glow peak maximum, as given in the well-established Randall-Wilkins equation (Equation 1)[41, 42, 43].

$$I(T) = n_0 \frac{s}{\beta} exp\left(-\frac{E}{kT}\right) exp\left[-\frac{s}{\beta}\int_{T_0}^{T} \exp(-\frac{E}{kT\prime})\, dT'\right] \qquad (1)$$

Where n_0 represents the initial amount of trapped charge carriers, s is the frequency factor, β is the constant heating rate, and E represents trap depth. The symbol k is the Boltzmann constant and T is the absolute temperature. T_0 indicates the starting temperature and T' represents a temperature variable and T is raised as a linear function of time, $T = T_0 + \beta t$. The specific values of trap depth can be fitted and calculated following Randall-Wilkins equation. As a simplification, the position of the TL peak maximum can be used to estimate the energy of trap depth (E_{trap}, in eV). If T_m represents the temperature for which the glow curve reaches a maximum, the related E_{trap} is approximately evaluated by using E_{trap} (eV) = $T_m/500$ (K). The estimated trap depth of $Sr_2SnO_4:Sm^{3+}, Si^{4+}$ pre-irradiated by X-rays is estimated to be 0.92 eV. It is worth mentioning that in order to obtain and compare E_{trap} for each persistent phosphor, the heating rate should be well considered. Upon Si substitution, the TL glow peak maximum was shifting to higher temperature and more deep-trap levels were formed in $Sr_2SnO_4:Sm^{3+},Si^{4+}$

sample, as observed in TL glow curves of Sr_2SnO_4:Sm^{3+} (Sm^{3+}-curve) and Sr_2SnO_4:Sm^{3+},Si^{4+} (Sm^{3+},Si^{4+}-curve). As a side note, all TL glow curves displayed in this work were not corrected with the thermal quenching profile (as discussed above in Figure S8). Therefore, in fact, there are more traps distributed in deep-lying energy levels and more electrons may populate traps of different trap depths. Also, the TL glow curve of Sr_2SnO_4:Sm^{3+} was compared with that after 10-minute fading at 70 °C, when most traps within Region-I were emptied (in Region I, the traps are relatively shallow, and are easily emptied during a long time fading at elevated temperature), and only traps with higher energy levels remained (Region-II and Region-III). Moreover, it could be observed that more traps with deeper-lying energy levels (Region-III) were present in the Sr_2SnO_4:Sm^{3+},Si^{4+} sample. These deep-lying trap distributions also contributed to the reddish-orange emitting persistent luminescence at higher temperatures (as shown in Figure S13). Furthermore, TL glow curves after X-ray irradiation for different durations were measured (Figure S14) and comparison of TL glow curves was made between Sr_2SnO_4:Sm^{3+} and Sr_2SnO_4:Sm^{3+},Si^{4+} phosphors in Figure 5(b). TL measurements started with a 10-minute fading after stopping the X-ray irradiation. Compared with UV charging, a stronger TL intensity was found after X-ray charging, suggesting more traps were charged by X-rays presumably due to a stronger absorption cross section in the case of high-energy X-ray charging[44]. Similar to that from UV charging, X-ray irradiation excited more deeper-lying traps in Sr_2SnO_4:Sm^{3+},Si^{4+}. Thus, the formation of deep-level traps in Sr_2SnO_4:Sm^{3+},Si^{4+} phosphor was experimentally confirmed. By chemical substitution strategy in this work, Sr_2SnO_4:Sm^{3+},Si^{4+} phosphor with deep-lying traps is excited by using UV and X-ray irradiation. All the energy from the deep-level traps can only be released upon thermal stimulation rather than ambient energy at room temperature[45].

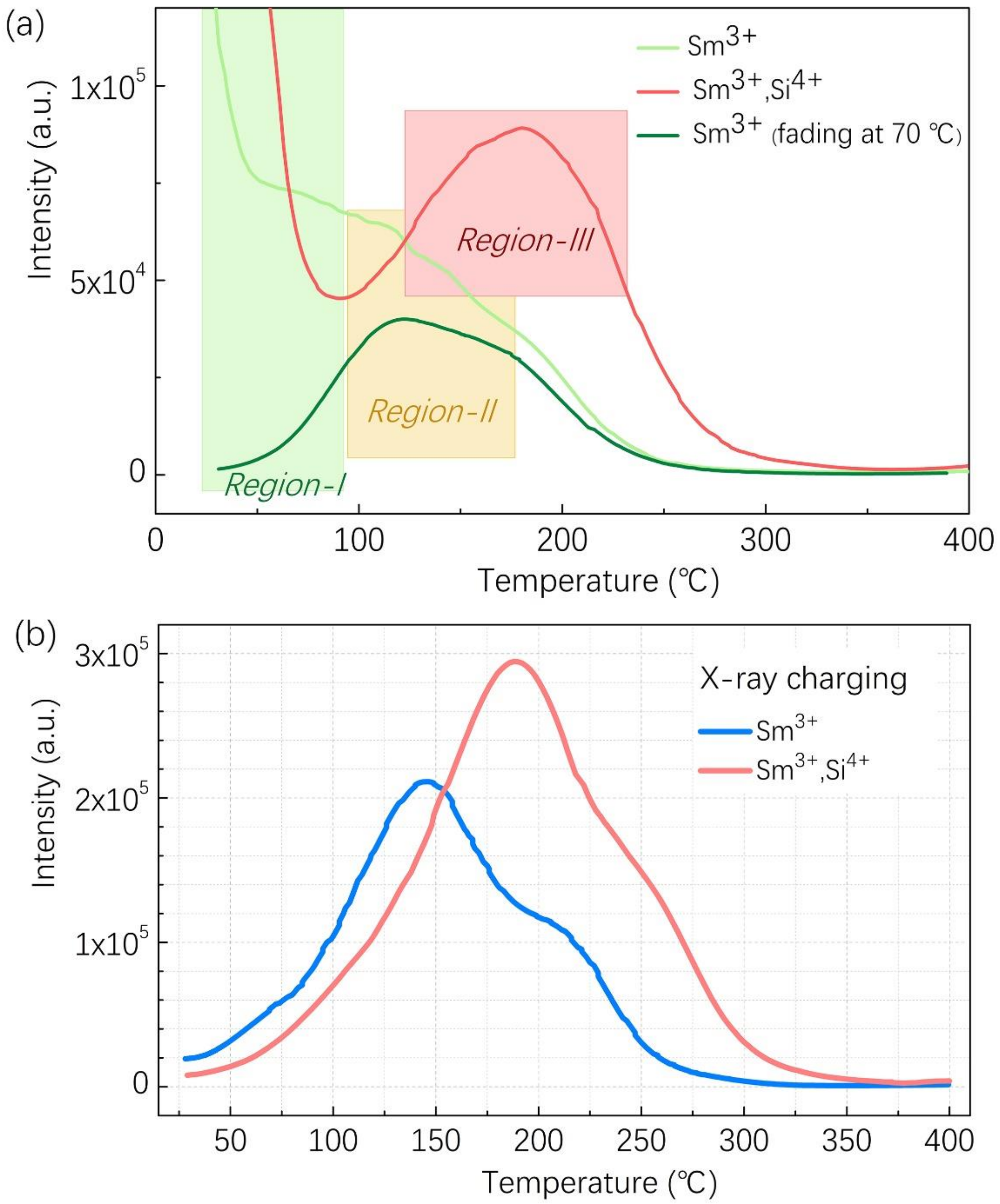

Figure 5. TL glow curves of $Sr_2SnO_4:Sm^{3+}$ and $Sr_2SnO_4:Sm^{3+},Si^{4+}$ after UV (a) and X-ray irradiation (70 kV, 1.5 mA) (b). For a clear illustration, three temperature regions (I-green, II-orange, III-red) were selected, and the TL glow curve of $Sr_2SnO_4:Sm^{3+}$ after fading at 70 °C was also shown in (a) for comparison.

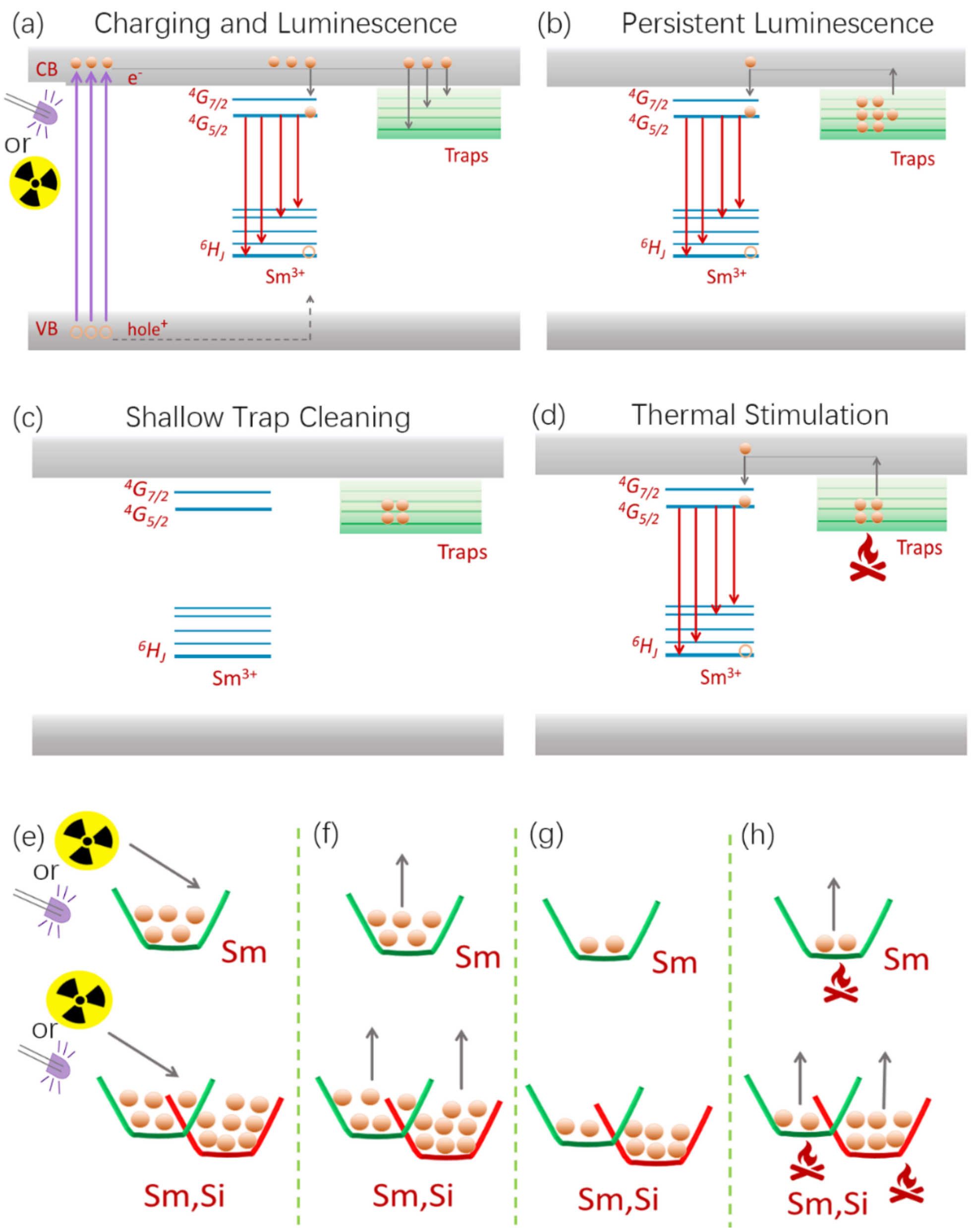

Figure 6. Proposed mechanism of persistent luminescence. (a) Charging step upon X-ray or UV excitation; (b) Persistent luminescence at room temperature; (c) Room-temperature trap cleaning after emptying shallow traps; (d) Thermally stimulated luminescence by external heating. Illustrations of trap information between Sr_2SnO_4:Sm^{3+} and Sr_2SnO_4:Sm^{3+},Si^{4+} samples during (e) X-ray or UV irradiation, (f) room temperature persistent luminescence, (g) the end of persistent luminescence, and (h) thermally stimulated luminescence upon external thermal stimulation.

Based on the results observed above, a possible mechanism of persistent luminescence is proposed and discussed in Figure 6. When excited by X-rays or UV light in the charging step, a large number of electrons are excited from the valence band (VB) to the conduction band (CB), resulting in the formation of electron-hole pairs. Upon X-ray irradiation, the high incident photon energy is dissipated by the creation of a whole cascade of high energy electrons, which ultimately leads to the creation of a large number of electron-hole pairs. Upon UV irradiation, single electron-hole pair are formed, as evident from the accordance between the host absorption spectrum[36] and the excitation spectrum (Figure S6). These excited electrons and holes can lead to steady state luminescence showing the typical emission lines from Sm^{3+} ions, as given in Figure 6(a). In parallel, the excited electrons (or holes) can be captured by traps with different energy levels within the host lattice. Considering the broad trap distributions observed from the TL measurements, the major traps responsible for persistent luminescence at room temperature are mostly located in Region-I (see Figure 5). Most of energy from the shallow traps (in Region-I) is released at room temperature, showing persistent luminescence in Figure 6(b). It should be mentioned that the shallow or deep traps are relatively speaking in the case of this work, and there is no strict definition. When it comes to Figure 6(c), no persistent luminescence is observed after a long-time de-trapping process. However, the absence of persistent luminescence does not mean there are no traps distributed in the host. In fact, most traps are still captured in deep-lying levels and they cannot be released at ambient temperature, when the thermal activation energy is insufficient. Alternatively, these deep-trapped electrons could be subsequently released at higher temperatures upon thermal stimulation, as illustrated in Figure 6(d). Comparison of trap information between $Sr_2SnO_4:Sm^{3+}$ and $Sr_2SnO_4:Sm^{3+},Si^{4+}$ samples was also made in Figure 6(e) to (h) during charging, persistent luminescence, the end of persistent luminescence and thermally stimulated luminescence upon external thermal stimulation, respectively. By Si substitution, the formation of deep-level traps contributed to the improvement of the stored energy, thus more energy could be released upon external thermal stimulation.

3.5. Rewritable Optical Data Storage and Information Encryption Applications

The Sr_2SnO_4:Sm^{3+},Si^{4+} phosphors exhibit both persistent luminescence and deep-trap storage capacity, which suggests a great promise in optical information storage and information encryption applications. Photographs of the emergency exit sign and “JNU” letters pieced together by Sr_2SnO_4:Sm^{3+},Si^{4+} phosphors were shown (Figure S15) during UV irradiation, after turning off the UV source with delay times of 5 s, 10 s, 60 s, and 600 s. After a long-time delay, the images became “invisible”. After thermal stimulation (up to 200 °C on a temperature-controlled heating platform), the hidden images were read out again. Furthermore, luminescent inks containing Sr_2SnO_4:Sm^{3+},Si^{4+} were used for practical optical data storage and readout application purpose. Text information of Chinese ideographs was printed on a piece of A4 paper by using screen-printing technique (see details in Experimental Section). In Figure 7, the printed information was hardly recognizable under daylight (a), but readable by naked eyes under 365 nm UV light (b). After ceasing the UV light, the printed information made of persistent phosphors can be recognized for a few minutes in the dark at room temperature, as shown in Figure 7(c-d) and Figure S16. With a long-time delay of 1 hour, the information was “invisible” on the paper (Figure 7(e)), which suggests optical information was stored (encryption). Subsequently, the paper was moved onto a heating platform preset at 150 °C, and the stored Chinese ideographs were reproduced and could be recorded easily by a cellphone camera (information readout, Figure 7(f)). More importantly, the encrypted optical information could also be decrypted by simply using a domestic electric hair drier (Figure S16). The initially hidden information was decrypted and clearly read out when heating the paper by the hair drier as illustrated in Figure 7(g) and (h). In contrast, only information of the heated area could show up (decryption), as observed in Figure 7(h) and Figure S16 with information decryption in right and left areas, respectively.

Based on photon trapping and de-trapping processes, optical information was easily rewritable and erasable on the paper by a commercially available 365 nm light emitting diode (information storage/encryption), and an electric hair drier (information readout/decryption). Figure 8 demonstrated the re-writability and erasability of the paper printed with luminescent inks. The encoded A4 paper could be bent or folded, but the information was covert among papers in ambient room-temperature condition under daylight or in darkness. The encoded optical information (Chinese ideographs or an emergency exit sign) was readable upon thermal stimulation as shown in Figure 8(a), Figure S17 (a) and (b). Notably, optical information could be repeatedly erased and written on the paper. Figure 8 (c) and Figure S17 (c) demonstrated the rewritable Chinese ideographs and emergency exit sign, respectively, on the paper with repeated information decryption. The encoded information was read out via either an electric hair drier or on a heating platform. The emission intensities upon read-out stage and after thermal cleaning were recorded as a function of cycle numbers (in Figure S18). The maximum read-out intensity kept relatively constant during different cycles. From the above results, the paper printed with luminescent inks exhibited excellent information re-writability and reusability, offering a great promise for rewritable optical information storage applications.

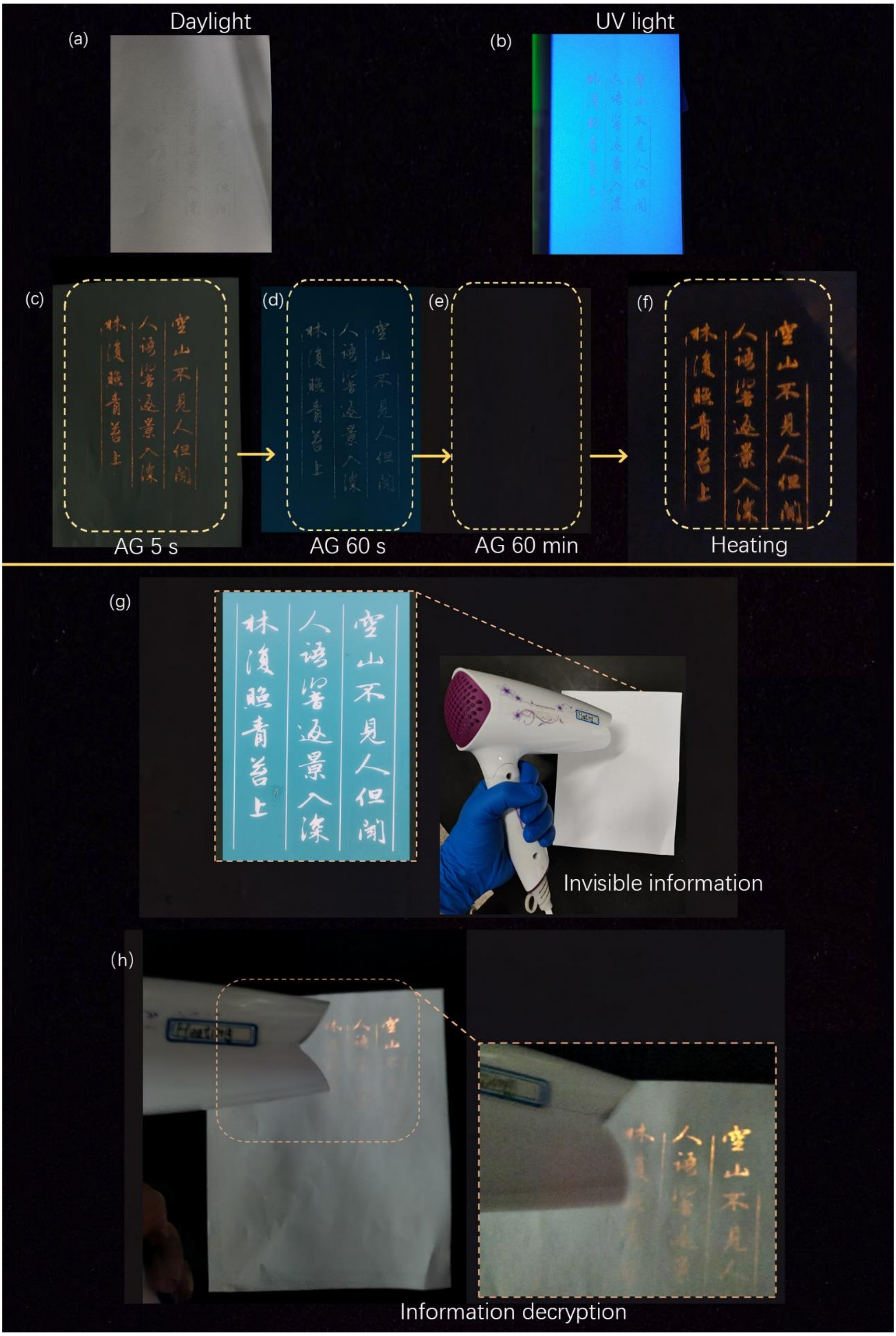

Figure 7. Applications for optical information storage and information decryption. Photographs of the paper printed with text information (Chinese ideographs) upon (a) daylight, or (b) UV light. After cessation of the irradiation, photographs of the emitting Chinese ideographs with a

delay time of 5 seconds (c), 60 seconds (d), 60 minutes (e), or under thermal stimulation (f). Information encryption on a paper (g), and the initially printed information was “invisible” after a long fading period. Optical information was read out (decryption) by an electric hair drier (h).

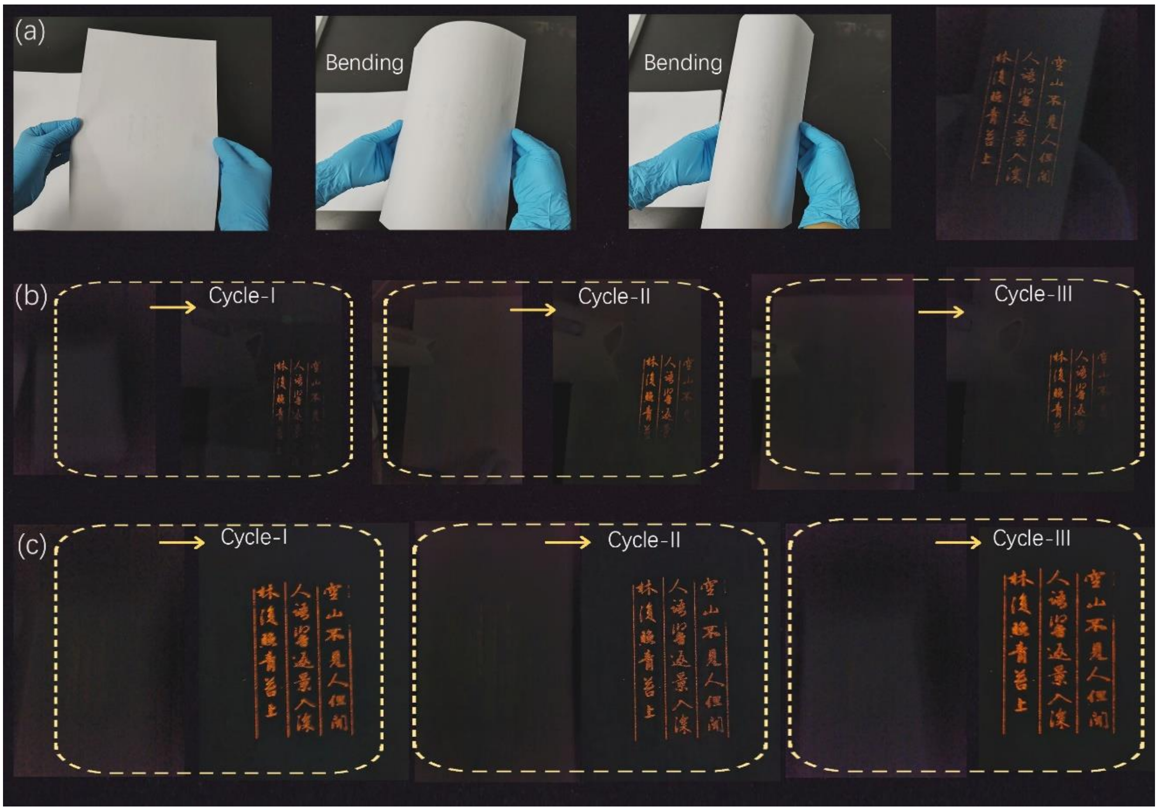

Figure 8. Rewritable information storage on the paper with repeated information encryption and decryption. (a) The encoded A4 paper was bent and the optical information was readable upon thermal stimulation. (b) and (c) Optical information was repeatedly erased and written on the paper. The information was read out via an electric hair drier (b) or on a heating platform (c) in three cycles, respectively.

4. Conclusions

In this work, deep-trap persistent luminescent materials with reddish-orange emissions and controllable photon release upon external stimulation were reported. Through substitution by Si, more and deeper trap levels were achieved in Sr_2SnO_4:Sm^{3+},Si^{4+} phosphors. Both ultraviolet light and high-energy X-ray irradiations could excite its reddish-orange emitting persistent luminescence. More importantly, rewritable optical data storage and readout based on photon trapping and de-trapping processes was demonstrated. Optical information could be repeatedly encoded by a commercially available 365 nm light emitting diode, and decoded handily upon thermal stimulation. The as-developed Sr_2SnO_4:Sm^{3+},Si^{4+} phosphors in this work not only show a great promise for rewritable optical information storage and data encryption, but also provide a good guidance to design other deep-trap-containing optical materials.

Supporting Information

Supporting Information is available from the author.

Acknowledgements

The authors acknowledge the financial support from the Natural Science Foundation of Jiangsu Province (No. BK20210481), Fundamental Research Fund of Jiangnan University (No. JUSRP122015) and National Natural Science Foundation of China (U1832110)

References

[1] X.-B. Li, N.-K. Chen, X.-P. Wang, H.-B. Sun, Phase-Change Superlattice Materials toward Low Power Consumption and High Density Data Storage: Microscopic Picture, Working Principles, and Optimization. *Advanced Functional Materials* **28**, 1803380 (2018); doi: 10.1002/adfm.201803380.

[2] C. S. Hwang, Prospective of Semiconductor Memory Devices: from Memory System to Materials. *Advanced Electronic Materials* **1**, 1400056 (2015); doi: 10.1002/aelm.201400056.

[3] S. V. Kalinin, B. G. Sumpter, R. K. Archibald, Big–deep–smart data in imaging for guiding materials design. *Nature Materials* **14**, 973-980 (2015); doi:10.1038/nmat4395.

[4] M. Gu, Q. Zhang, S. Lamon, Nanomaterials for optical data storage. *Nature Reviews Materials* **1**, 16070 (2016); doi:10.1038/natrevmats.2016.70.

[5] Y. Lu, J. Zhao, R. Zhang, Y. Liu, D. Liu, E. M. Goldys, X. Yang, P. Xi, A. Sunna, J. Lu, Y. Shi, R. C. Leif, Y. Huo, J. Shen, J. A. Piper, J. P. Robinson, D. Jin, Tunable lifetime multiplexing using luminescent nanocrystals. *Nature Photonics* **8**, 32-36 (2014); doi:10.1038/nphoton.2013.322.

[6] Y. Zhuang, Y. Lv, L. Wang, W. Chen, T. Zhou, T. Takeda, N. Hirosaki, R.-J. Xie, Trap Depth Engineering of $SrSi_2O_2N_2:Ln^{2+},Ln^{3+}$ (Ln^{2+}= Yb, Eu; Ln^{3+}= Dy, Ho, Er) Persistent Luminescence Materials for Information Storage Applications. *ACS Applied Materials & Interfaces* **10**, 1854-1864 (2018); doi:10.1021/acsami.7b17271.

[7] Y. Zhuang, L. Wang, Y. Lv, T. L. Zhou, R. J. Xie, Optical Data Storage and Multicolor Emission Readout on Flexible Films Using Deep-Trap Persistent Luminescence Materials. *Advanced Functional Materials* **28**, 1705769 (2018); doi:10.1002/adfm.201705769

[8] D. Liu, L. Yuan, Y. Jin, H. Wu, Y. Lv, G. Xiong, G. Ju, L. Chen, S. Yang, Y. Hu, Tailoring Multidimensional Traps for Rewritable Multilevel Optical Data Storage. *ACS Applied Materials & Interfaces* **11**, 35023-35029 (2019); doi:10.1021/acsami.9b13011.

[9] W. Li, Y. Zhuang, P. Zheng, T.-L. Zhou, J. Xu, J. Ueda, S. Tanabe, L. Wang, R.-J. Xie, Tailoring Trap Depth and Emission Wavelength in $Y_3Al_{5-x}Ga_xO_{12}:Ce^{3+},V^{3+}$ Phosphor-in-Glass Films for Optical Information Storage. *ACS Applied Materials & Interfaces* **10**, 27150-27159 (2018); doi:10.1021/acsami.8b10713.

[10] Z. Pan, Y.-Y. Lu, F. Liu, Sunlight-activated long-persistent luminescence in the near-infrared from Cr^{3+}-doped zinc gallogermanates. *Nature Materials* **11**, 58 (2012); doi:10.1038/nmat3173.

[11] T. Maldiney, A. Bessière, J. Seguin, E. Teston, S. K. Sharma, B. Viana, A. J. Bos, P.

Dorenbos, M. Bessodes, D. Gourier, D. Scherman, C. Richard, The in vivo activation of persistent nanophosphors for optical imaging of vascularization, tumours and grafted cells. *Nature Materials* **13**, 418 (2014); doi:10.1038/nmat3908.

[12] J. Miranda de Carvalho, C. C. S. Pedroso, I. P. Machado, J. Hölsä, L. C. V. Rodrigues, P. Głuchowski, M. Lastusaari, H. F. Brito, Persistent luminescence warm-light LEDs based on Ti-doped RE_2O_2S materials prepared by rapid and energy-saving microwave-assisted synthesis. *Journal of Materials Chemistry C* **6**, 8897-8905 (2018); doi:10.1039/C8TC01826J.

[13] P. Pei, Y. Chen, C. Sun, Y. Fan, Y. Yang, X. Liu, L. Lu, M. Zhao, H. Zhang, D. Zhao, X. Liu, F. Zhang, X-ray-activated persistent luminescence nanomaterials for NIR-II imaging. *Nature Nanotechnology* **16**, 1011-1018 (2021); doi:10.1038/s41565-021-00922-3.

[14] Y. Zhuang, D. Chen, W. Chen, W. Zhang, X. Su, R. Deng, Z. An, H. Chen, R.-J. Xie, X-ray-charged bright persistent luminescence in $NaYF_4:Ln^{3+}@NaYF_4$ nanoparticles for multidimensional optical information storage. *Light: Science & Applications* **10**, 132 (2021); doi:10.1038/s41377-021-00575-w.

[15] D. Poelman, D. V. d. Heggen, J. Du, E. Cosaert, P. F. Smet, Persistent phosphors for the future: Fit for the right application. *Journal of Applied Physics* **128**, 240903 (2020); doi:10.1063/5.0032972.

[16] S. Lin, H. Lin, C. Ma, Y. Cheng, S. Ye, F. Lin, R. Li, J. Xu, Y. Wang, High-security-level multi-dimensional optical storage medium: nanostructured glass embedded with $LiGa_5O_8:Mn^{2+}$ with photostimulated luminescence. *Light: Science & Applications* **9**, 22 (2020); doi:10.1038/s41377-020-0258-3.

[17] F. Liu, W. Yan, Y.-J. Chuang, Z. Zhen, J. Xie, Z. Pan, Photostimulated near-infrared persistent luminescence as a new optical read-out from Cr^{3+}-doped $LiGa_5O_8$. *Scientific Reports* **3**, 1554 (2013); doi:10.1038/srep01554.

[18] X. Ou, X. Qin, B. Huang, J. Zan, Q. Wu, Z. Hong, L. Xie, H. Bian, Z. Yi, X. Chen, Y. Wu, X. Song, J. Li, Q. Chen, H. Yang, X. Liu, High-resolution X-ray luminescence extension imaging. *Nature* **590**, 410-415 (2021); doi:10.1038/s41586-021-03251-6.

[19] J. Qiao, G. Zhou, Y. Zhou, Q. Zhang, Z. Xia, Divalent europium-doped near-infrared-emitting phosphor for light-emitting diodes. *Nature Communications* **10**, 5267 (2019); doi:10.1038/s41467-019-13293-0.

[20] Z. Yang, Y. Zhou, J. Qiao, M. S. Molokeev, Z. Xia, Rapid Synthesis of Red-Emitting $Sr_2Sc_{0.5}Ga_{1.5}O_5:Eu^{2+}$ Phosphors and the Tunable Photoluminescence Via Sr/Ba Substitution. *Advanced Optical Materials* **9**, 2100131 (2021); doi:

10.1002/adom.202100131.

[21] Y. Zhao, J. Du, X. Wu, Y. Wang, D. Poelman, Enhanced near-infrared persistent luminescence in $MgGa_2O_4:Cr^{3+}$ through codoping. *Journal of Luminescence* **220**, 117035 (2020); doi:10.1016/j.jlumin.2020.117035.

[22] J. Du, D. Poelman, Near-infrared persistent luminescence in Mn^{4+} doped perovskite type solid solutions. *Ceramics International* **45**, 8345-8353 (2019); doi:10.1016/j.ceramint.2019.01.142.

[23] J. Ueda, S. Miyano, S. Tanabe, Formation of Deep Electron Traps by Yb^{3+} Codoping Leads to Super-Long Persistent Luminescence in Ce^{3+}-Doped Yttrium Aluminum Gallium Garnet Phosphors. *ACS Applied Materials & Interfaces* **10**, 20652-20660 (2018); doi:10.1021/acsami.8b02758.

[24] M. Zhao, Z. Yang, L. Ning, Z. Xia, Tailoring of White Luminescence in a $NaLi_3SiO_4:Eu^{2+}$ Phosphor Containing Broad-Band Defect-Induced Charge-Transfer Emission. *Advanced Materials* **33**, 2101428 (2021); doi:10.1002/adma.202101428.

[25] T. Hu, L. Ning, Y. Gao, J. Qiao, E. Song, Z. Chen, Y. Zhou, J. Wang, M. S. Molokeev, X. Ke, Z. Xia, Q. Zhang, Glass crystallization making red phosphor for high-power warm white lighting. *Light: Science & Applications* **10**, 56 (2021); doi:10.1038/s41377-021-00498-6.

[26] O. Q. De Clercq, D. Poelman, Local, temperature-dependent trapping and detrapping in the $LiGa_5O_8:Cr$ infrared emitting persistent phosphor. *ECS Journal of Solid State Science and Technology* **7**, R3171-R3175 (2018); doi:10.1149/2.0211801jss.

[27] M. Allix, S. b. Chenu, E. Véron, T. Poumeyrol, E. A. Kouadri-Boudjelthia, S. Alahrache, F. Porcher, D. Massiot, F. Fayon, Considerable improvement of long-persistent luminescence in germanium and tin substituted $ZnGa_2O_4$. *Chemistry of Materials* **25**, 1600-1606 (2013); doi:10.1021/cm304101n.

[28] Y. Zhuang, J. Ueda, S. Tanabe, Enhancement of red persistent luminescence in Cr^{3+}-doped $ZnGa_2O_4$ phosphors by Bi_2O_3 codoping. *Applied Physics Express* **6**, 052602 (2013); doi:10.7567/APEX.6.052602.

[29] M. Deng, Q. Liu, Y. Zhang, C. Wang, X. Guo, Z. Zhou, X. Xu, Novel Co-Doped $Y_2GeO_5:Pr^{3+},Tb^{3+}$: Deep Trap Level Formation and Analog Binary Optical Storage with Submicron Information Points. *Advanced Optical Materials* **9**, 2002090 (2021); doi: 10.1002/adom.202002090.

[30] L. Bing-Fu, Y. Song, Z. Yong-Zhe, L. Ying-Liang, Luminescence Properties of $Sr_2SnO_4:Sm^{3+}$ Afterglow Phosphor. *Chinese Physics Letters* **27**, 037201 (2010);

doi:10.1088/0256-307x/27/3/037201.

[31] S. Kamimura, H. Yamada, C.-N. Xu, Strong reddish-orange light emission from stress-activated $Sr_{n+1}Sn_nO_{3n+1}$:Sm^{3+} (n = 1, 2, ∞) with perovskite-related structures. *Applied Physics Letters* **101**, 091113 (2012); doi:10.1063/1.4749807.

[32] R. Yu, N. Xue, T. Wang, Z. Zhao, J. Wang, Z. Hei, M. Li, H. Mi Noh, J. Hyun Jeong, Photoluminescence characteristics of high thermal stable fluorosilicate apatite $Ba_2Y_3(SiO_4)_3F$:Sm^{3+} orange-red emitting phosphor. *Ceramics International* **41**, 6030-6036 (2015); doi:10.1016/j.ceramint.2015.01.046.

[33] J. Tang, P. Du, W. Li, G. Yuan, Z. Liu, L. Luo, The integration of diverse fluorescence performances of $Sr_{2-x}SnO_4$:xSm^{3+} ceramics with an infinite luminescence modulation ratio. *Chemical Engineering Journal* **410**, 128287 (2021); doi:10.1016/j.cej.2020.128287.

[34] W. F. Hornyak, R. Chen, Thermoluminescence and phosphorescence with a continuous distribution of activation energies. *Journal of Luminescence* **44**, 73-81 (1989); doi:10.1016/0022-2313(89)90023-9.

[35] O. Q. De Clercq, J. Du, P. F. Smet, J. J. Joos, D. Poelman, Predicting the afterglow duration in persistent phosphors: a validated approach to derive trap depth distributions. *Physical Chemistry Chemical Physics* **20**, 30455-30465 (2018); doi:10.1039/C8CP06139D.

[36] C. Wang, Z. Zheng, Y. Zhang, Q. Liu, M. Deng, X. Xu, Z. Zhou, H. He, Modulating trap properties by Nd^{3+}-Eu^{3+} co-doping in Sr_2SnO_4 host for optical information storage. *Optics Express* **28**, 4249-4257 (2020); doi:10.1364/OE.386164.

[37] S. Kamimura, H. Yamada, C.-N. Xu, Purple photochromism in Sr_2SnO_4:Eu^{3+} with layered perovskite-related structure. *Applied Physics Letters* **102**, 031110 (2013); doi:10.1063/1.4788752.

[38] Y. Zhang, L. Luo, K. Li, W. Li, Y. Hou, Reversible up-conversion luminescence modulation based on UV-VIS light-controlled photochromism in Er^{3+} doped Sr_2SnO_4. *Journal of Materials Chemistry C* **6**, 13148-13156 (2018); doi:10.1039/C8TC04725A.

[39] J. Tang, Y. Mu, P. Du, L. Luo, Luminescence modulation of the Eu^{3+} doped $Sr_{n+1}Sn_nO_{3n+1}$ (n=1, 2, 5, ∞) ceramics based on photochromism and its application in anti-counterfeiting technology. *Ceramics International* **46**, 11962-11969 (2020); doi:10.1016/j.ceramint.2020.01.235.

[40] Z. Yang, J. Du, L. I. D. J. Martin, D. Van der Heggen, D. Poelman, Highly Responsive Photochromic Ceramics for High-Contrast Rewritable Information Displays. *Laser & Photonics Reviews* **15**, 2000525 (2021); doi:10.1002/lpor.202000525.

[41] A. J. J. Bos, Thermoluminescence as a Research Tool to Investigate Luminescence

Mechanisms. *Materials* **10**, 1357 (2017); doi:10.3390/ma10121357.

[42] J. T. Randall, M. H. F. Wilkins, Phosphorescence and electron traps-I. The study of trap distributions. *Proc. R. Soc. Lond. A* **184**, 365-389 (1945); doi:10.1098/rspa.1945.0024.

[43] J. T. Randall, M. H. F. Wilkins, Phosphorescence and electron traps II. The interpretation of long-period phosphorescence. *Proc. R. Soc. Lond. A* **184**, 390-407 (1945); doi:10.1098/rspa.1945.0025.

[44] J. Du, K. Li, R. Van Deun, D. Poelman, H. Lin, Near-Infrared Persistent Luminescence and Trap Reshuffling in Mn^{4+} Doped Alkali-Earth Metal Tungstates. *Advanced Optical Materials* **10**, 2101714 (2022); doi:10.1002/adom.202101714.

[45] J. Du, A. Feng, D. Poelman, Temperature Dependency of Trap-Controlled Persistent Luminescence. *Laser & Photonics Reviews* **14**, 2000060 (2020); doi:10.1002/lpor.202000060.

Graphical abstract

Through substitution by Si, persistent luminescent materials with reddish-orange emissions and deep-level traps are achieved in Sr_2SnO_4:Sm^{3+},Si^{4+} phosphors. Based on photon trapping and de-trapping processes, information can be encoded by UV light/X-ray and decoded upon thermal stimulation. The as-developed material in this work shows a great promise for rewritable optical information storage and data encryption.